10-2-1979

Moire fringe measurements of corneal analogues

James A. Edwards
Pacific University

Moire fringe measurements of corneal analogues

Abstract

Moire fringe measurements of corneal analogues

Degree Type

Thesis

Degree Name

Master of Science in Vision Science

Committee Chair

Jurgen R. Meyer-Arendt

Subject Categories

Optometry

MOIRÉ FRINGE MEASUREMENTS OF CORNEAL ANALOGUES

by,
James A. Edwards

Pacific University College of Optometry
October 2, 1979

MOIRÉ FRINGE MEASUREMENTS OF CORNEAL ANALOGUES

Midterm grade A

Final grade A

This paper has been approved by,

J.R. Meyer-Arendt

Dr. Jurgen R. Meyer-Arendt, Advisor

in satisfaction of the thesis requirement for

the Doctor of Optometry degree

October 2, 1979

ACKNOWLEDGEMENTS

I wish to express appreciation to Dr. Jurgen R. Meyer-Arendt and to the Pacific University College of Optometry for providing the equipment and facilities that made this study possible.

TABLE OF CONTENTS

I. Introduction 1-2

II. Methods 3-10

a) Figure 1 - Theoretical design 3

b) Figure 2 - Experimental design 4

c) Table 1 - Relative magnification of reference 7

d) Table 2 - Relative magnification of test lens 7

e) Figure 3 - Relative magnification range 8

f) Figure 4 - Calibration graph 10

g) Table 3 - Experimental findings 9

h) Figure 5 - Experimental observations 10

III. Discussion 11-14

a) Figure 6 - Moiré device adapted to a biomicroscope 13

IV. References 15

V. Index - Raw data 16-17

ABSTRACT

A method of measuring the anterior radius of curvature of contact lenses utilizing the summation classification of Moiré fringes is described. An accuracy of .03 mm radius of curvature is obtained from measurements on corneal analogues of 7.78, 8.14, and 8.46 mm radius of curvature. Suggestions are offered to adapt this method to human corneal application.

Moiré Fringe Measurements of Corneal Analogues

Introduction:

The analysis of the human cornea is traditionally considered from both quantitative and qualitative perspectives. The most commonly employed instrument for corneal analysis is the keratometer which utilizes geometrical optics in determining the radius of curvature passing through two points in each of two principal meridians of the cornea. Qualitative assessment is made on the basis of overall shape of the corneal image and on "distortions" seen as vernier displacements of the borders within the corneal image.

The concept of a "new metrology" has been used to describe the progress that has been made within the last 50 years in precision surface measurement techniques.[1] The applications of this "new metrology" in the physical sciences have involved both interferometric and moiré pattern analysis. Interferometric methods as used in physical optics presently set the limits of measurement accuracy. The accuracy of interferometric instruments is dependent upon the wavelength of light used. This relationship is not necessarily due to the inherent nature of light waves and optics but instead it is a characteristic of the method of pattern analysis. Pattern analysis is also the method used in geometrical optics when Ronchi rulings are transposed by inhomogeneous optical media. These methods of optical measurement are known as schlieren devices and have been used in microscopy to analyze the smooth reflective surfaces of cell structures. During schlieren analysis, observations are reported as vernier displacements in the live pattern produced by reflective surfaces.[2] When the optical system used for surface analysis is designed to maximize the sensitivity of the instrument to vernier displacements of the borders within the image formed by geometrical optics, moiré fringe production is the preferred method. Ronchi rulings have been used in assessing the angular rotation of reflective surfaces. Such moiré techniques have been shown to provide a versatile apparatus for surface analysis. Accuracy in the order of wavelengths of light, as is realized

using interferometric techniques is compromised to provide a wider range of surfaces which can be examined without readjustment of the instrument. Also, the materials required for moiré techniques are inexpensively obtainable in contrast to interferometric methods.

The first to accurately describe how moiré patterns are produced was Raleigh in 1874. Oster has hade a thorough analysis of moiré fringe patterns produced by combining various lined pattern. He describes moiré fringes as "the loci of intersections of two overlapping figures."[4] Moiré patterns have been classified into two types. The multiplication type is such that one pattern is modulated by the reflectance or transmittance of the other pattern. The summation type combines the intensity distribution of two patters in an additive process to produce fringes.[5]

Detailed analyses of moiré patterns as applied to surfaces of textiles, coins and mannequins have been reported. The most widely used type of moiré pattern is the multiplication type. The equipment required for accurate analysis is fairly cumbersome becouse it requires a large illumination system and careful photographic pattern analysis.[6] The summation class of fringes has also been utilized in analysing surfaces. This technique provides a more compact apparatus but still requires photographic analysis.[7] An instrument has been described which uses the multiplication class of moiré fringes to directly assess the surface characteristics of contact lenses.[8]

Techniques in moiré pattern analysis as applied to human corneal topography have been described in the literature. A multiplication technique has been designed utilizing parallel lines and photographic superimposition to produce the desired effect with an accuracy of 1.45%, measuring a steel ball of 13.85 mm radius of curvature.[9] Mandell has also reported a method of utilizing the moiré phenomena while directly assessing corneal topography.[10]

Presently, the major difficulties in corneal applications of moiré surface analysis are 1)experimental design - apparatus stability, range of applicability and material costs, 2)optical alignment of illumination and observation systems providing the

conditions necessary for moiré fringes to correspond to contour lines in qualitative assessments and, 3) visibility of fringes produced. These areas are of principal interest in the study of moiré applications. When these factors are maximized, corneal topography seems promising. In this study I have considered some of the basic design features of moiré techniques as applied to measurements on the human cornea.

Methods:

The type of moiré production used in this study is of the summation class of fringes. To obtain the necessary division and recombination of the intensity distribution in the Ronchi ruling used as a target, a cube beam splitter is used. Figure 1 illustrates the progression of light from left to right through the optical elements when the cornea (a convex mirror) is considered to have -250.00 D power. At the top of figure 1, the vergence of light, in diopters, as it passes through each interface is given. Below, the power of each optical component, in diopters, and distances, in mm, are given. The index of refraction of the cube is 1.515. The symbols represent: G-grating, B-beam splitter, L- lens, C-cornea, O-objective, R-reticle, E-eyepiece.

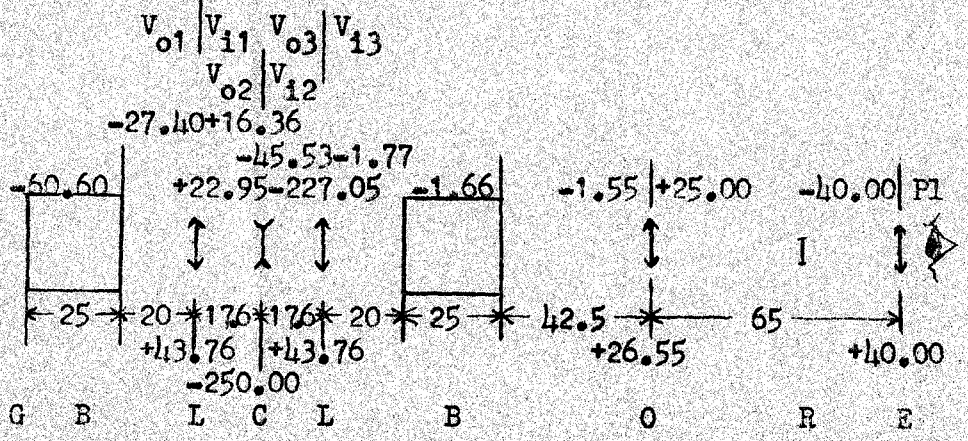

Figure 1

Figure 2 is a drawing of the experimental arrangement. As it can be seen, two images are formed in the plane of the reticle by combining the light reflected from two contact lenses (serving as corneal analogues). It is in the plane of the reticle that the moiré fringes are observed and measured. These fringes are characteristic of the lenses' powers and positions, the analogues' reflective powers and positions, and the objective and eyepiece powers and positions. The objective, eyepiece and one of the lenses are held in constant position. The powers of both lenses and the anterior radius of curvature of one of the analogues are known. When the analogue of known power is located behind the lens of variable position and a moiré fringe of constant width is maintained in the reticle, the position of the lens of variable position is proportional to the radius of curvature of the analogue of unknown power located behind the lens of constant position.

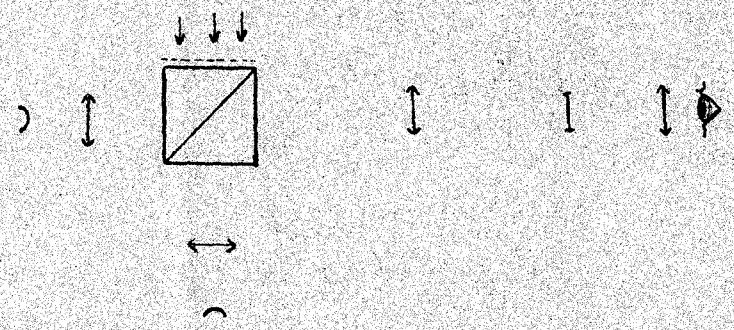

Figure 2

The powers of the lenses and analogues and the fringe width determine the distances between the optical elements. The powers of the elements are chosen therefore to minimize the overall size of the apparatus while utilizing a fringe width that is well visible in the telescope. The powers of the analogues are chosen to correspond to typical human corneas. Both lenses have approximatly the same power to simplify the mathematical treatment of the data obtained.

Due to the short distances between the optical elements, precise measurement of

the parameters of the lenses, analogues and beam splitter must be made. Calipers were used to verify the center and edge thickness of the lenses and the thickness of the beam splitter ($\pm$ .1 mm). A transparent ruler was used to verify the front and back vertex powers of the lenses by autocollimation ($\pm$ .5 mm). The anterior radius of curvature of the contact lenses were measured with a spherometer ($\pm$ .05 mm). The location of the lens of constant position (test lens) was measured using a transparent ruler. The location of the lens of variable position (reference lens) was measured using a transparent ruler in combination with a screw type carriage adapted from an interferometer ($\pm$ .001 mm). The reticle consisted of a scale of 50 one-unit divisions. The carriage had a range (measured in mm distance between the back surface of the beam splitter and the principal plane of the lens) of 10 to 35 mm.

To align the instrument, the reference lens is first placed at the 10 mm position. An opaque shield blocks light reflected from the test lens. The reference analogue is brought from far to near with respect to the reference lens for fine adjustment. The observer has to keep the reticle in focus while adjusting the lenses. The lens position and tilt are then varied until an evenly illuminated image of the target grating is centered in the scale of the reticle. The carriage is then moved to the 35 mm position and the image is fine-focused by moving the analogue from far to near. The images produced from both positions must be centered in the reticle scale for the measurements to be useful when calibrating the instrument. Once this is done, the opaque shield is moved to block the reflections from the reference lens. The image produced by the reflection from the test analogue is then fine-focused and centered on the reticle scale in the same fashion as the reference analogue is adjusted. The opaque shield is then removed and moiré fringes are seen. If the fringes are asymmetric, the test analogue is adjusted until the fringe pattern is symmetrical with respect to the reticle scale. This adjustment includes rotation of the test analogue. The fringe width is measured in terms of reticle scale units. Measurements

are made in the central region of the scale to minimize the effect of aberrations. The position of the reference lens is varied while fine-focusing with the reference analogue. The position of the reference lens (when the fringe separation is 10 units) determines the anterior radius of curvature of the test analogue. A graph can then be drawn with the position of the reference lens plotted as the ordinate and the radius of curvature of the test analogue as the abscissa. The anterior radius of curvature of the unknown surface can then be extrapolated from the graph once the position of the reference lens corresponding to a fringe width of 10 units is determined.

The moiré fringes produced in the plane of the reticle are the result of differing line separations in each of the two images. This difference is expressed by the magnification of each of the grating images relative to the reticle scale. When the reference lens and the analogue are positioned such that the line spacing within the resultant image is equal to one reticle scale unit, the position of the lens is noted as the position of unit magnification (m_{TO}) with respect to the reticle scale. Using geometrical optics, the total magnification of this image with respect to the Ronchi ruling is given by the vergence ratios at each of the interfaces of the system. When the lens power and position are known and the entrance and exit vergence is held constant (with respect to the beam splitter surface) by maintaining a constant telescope magnification and target grating position, the only remaining variable is the distance, X, between the reference analogue and the principal plane of the reference lens. This distance can be determined for any position of the reference lens by solving for X in the following equation:

$$V_{i2} - I = \frac{\frac{V_{i1}}{1 - V_{i1}X} - C}{1 - \left(\frac{V_{i1}}{1 - V_{i1}X} - C\right)X} \qquad \text{Equation 1}$$

When the reference lens is in the position providing unit magnification, the above

equation yields X and the vergence of light at each interface is determined. These vergences are related to the total magnification, m_T, by the following relationship:

$$\frac{V_{o1} \times V_{o2} \times V_{o3}}{V_{i1} \times V_{i2} \times V_{i3}} = m_T \qquad \text{Equation 2}$$

In this study, when unit magnification was obtained, X = 76.3 mm. To determine the relative magnification range of the instrument, the total magnification was calculated for reference lens settings of 76.3, 43, and 10 mm. These total magnifications are converted to relative magnifications (corresponding to the direct reticle scale measurements) using the relationship:

$$m_{Rn} = \frac{m_{Tn}}{m_{TO}} \qquad \text{Equation 3}$$

The values obtained for m_{TO}, m_{Tn}, and m_{Rn} are shown in Table 1. These values correspond to an anterior radius of curvature of the test surface of 7.45 mm, and a reference lens power of +43.761 D. Then X is calculated using Equation 1. The exit vergence is held at -1.66 D.

n	m_{Tn}	m_{Rn}	X_n
76.3	2.867	1.000	16.737
43	3.580	1.245	17.338
10	4.241	1.474	18.158

Table 1

i	m_{Ti}	m_{Ri}	X_i
7.78	4.352	1.513	17.590
8.14	4.550	1.582	17.379
8.46	4.726	1.643	17.191

Table 2

In figure 3 a graph is shown which demonstrates the relative magnification range of the instrument used in this study. The ordinate is representative of the relative magnification. The abscissa represents the position of the reference lens with respect to the beam splitter surface.

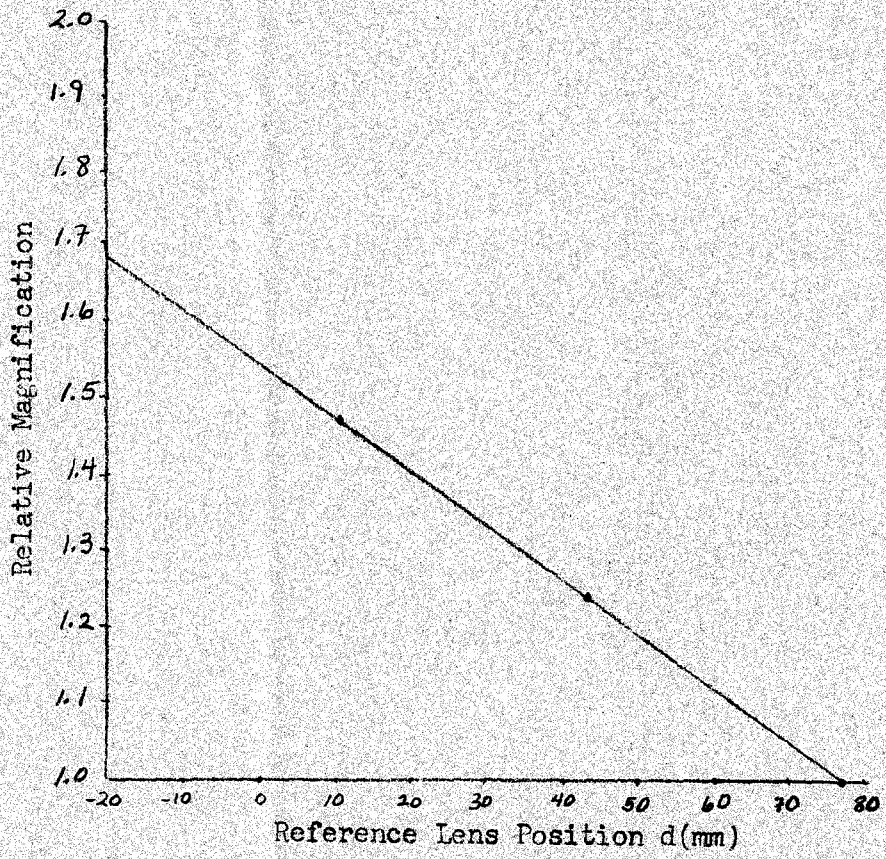

Figure 3

When considering the relationship between relative magnification and the radius of curvature of the test surface, equation 1 can again be used to determine X and therefore the vergences used in equation 2, yielding the total magnification produced by the test lens. These values are converted to reticle scale units by using m_{TO} in equation 3 as I have done in table 1.

Three test surfaces were used in this study. The radii of curvature were 7.78, 8.14, and 8.46 mm. The test lens was determined to be +44.091 D located

at a constant 17.680 mm from the beam splitter surface. The total and relative magnifications and the corresponding X value as calculated are shown in Table 2.

The equation for moiré fringe separation when two patterns of parallel lines of variable spacing are superimposed, consists of two factors. The first factor varies with the line separation and is shown in equation 4a. The second factor varies with the angle, θ, between the overlapping lines within the two grating images. This is shown in equation 4b where d = moiré fringe separation and Ψ = angle between the resultant moiré fringe and the axis of the reference image.

$$d = \frac{m_{Ri}\, m_{Rn}}{\left[m_{Ri}^{2} + m_{Rn}^{2} - 2m_{Ri}\, m_{Rn}\right]^{\frac{1}{2}}} \qquad (a)$$

$$\sin \Psi = \frac{m_{Rn} \sin \theta}{\left[m_{Ri}^{2} + m_{Rn}^{2} - 2m_{Ri}\, m_{Rn} \cos\theta\right]^{\frac{1}{2}}} \qquad (b)$$

Equation 4

The technique for measuring fringe width described above requires neutralizing the θ factor in equation 4b. Therefore, when m_{Ri} is calculated for the test surfaces chosen in this study, and a fringe spacing, d, of 10 reticle units is desired, the theoretically predicted m_{Rn} is obtained from equation 4a and the appropriate reference lens position is extrapolated from figure 3. These calculated reference lens positions are plotted in figure 4 as the ordinate. The abscissa in this figure represents the radius of curvature of the test surfaces used. The graph in figure 4 (denoted by x's) represents the theoretically predicted reference lens positions for the test surfaces used.

r_i	$\bar{d}$	σ
7.78	30.288	.565
8.14	23.286	.584
8.46	17.118	.639

Table 3

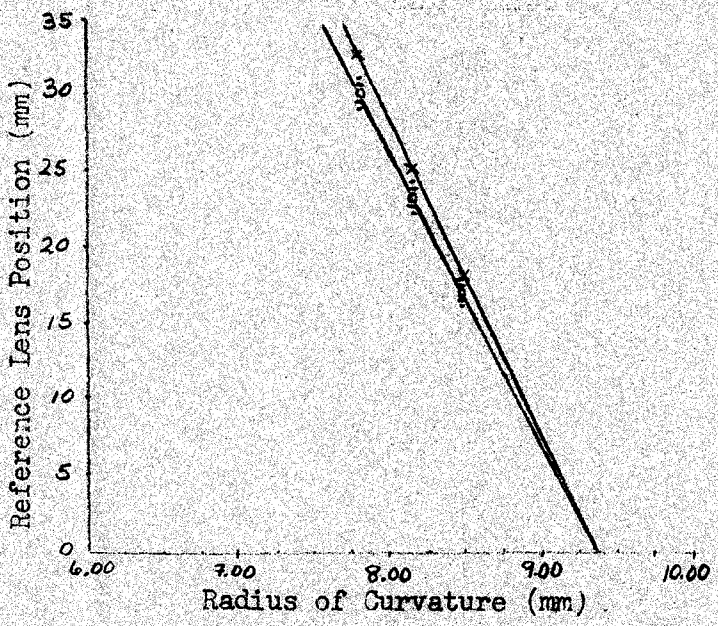

Figure 4

The instrument is aligned and fine focused as described above. When the test surface is in its proper position, 20 readings were taken. Then readings were taken by moving the reference lens from a distant to near position with respect to the beam splitter surface and 10 readings were taken by moving the reference lens from a near to distart position. Fine-focusing as described above was always used before reticle measurements were made. The mean and standard deviation were then determined for each test surface as shown in table 3. These findings are plotted in figure 4 (denoted by o's). The observations made during alignment and measurement are illustrated below in figure 5:a)test image, b)reference image, c)moiré fringe pattern.

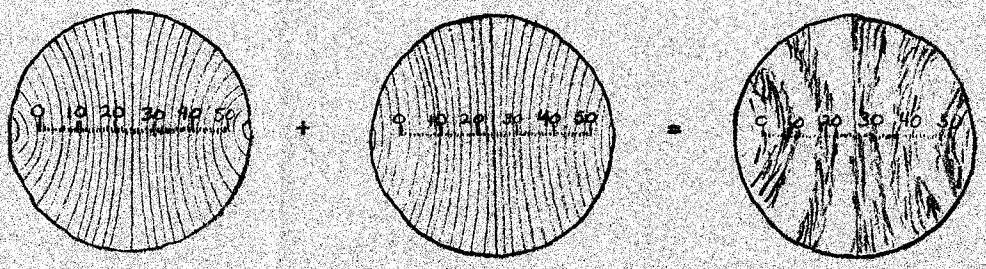

(a) (b) (c)

Figure 5

Discussion:

As can be seen from figure 4, the experimental graph does not fully match the theoretically predicted graph. The experimental data differ slightly in both placement and slope (19.368 mm/mm radius of curvature vs. the theoretically predicted 20.735 mm/mm radius of curvature). Many factors may have contributed to this deviation. The apparatus is extremely sensitive to lens position and image alignment. When a difference of .5 mm in the test lens position is considered in the theoretical calculations, the theoretical graph moves up or down to an extent large enough to explain the disparity between the two graphs. Even if such an error is not entirely due to the test lens position, a combination of errors could bring about the same result. The deviation of the slope is probably due to a slight misalignment of the two images when superimposed in the telescope reticle. Careful calibration of the instrument before making any measurements will minimize this error. Some error of observation is demonstrated by the distribution represented in the standard deviation increments in the experimental findings of figure 4.

The repeatability of this method is dependent upon the stability of construction. Constant relationships between the optical elements must be maintained. This would be relatively easy to do. For instance, the test lens could be cemented to the beam splitter. This would eliminate four reflections and increase the structural rigidity. The movable carriage used with the reference lens proved to be of dependable construction. The reference surfaces, finally, could be made more stable than using a conventional contact lens.

As mentioned earlier, the major difficulties encountered in this technique are alignment, construction, and visibility of the fringes. Utilizing the cube beam splitter to produce the summation class of moiré fringes minimizes the first two factors at the expense of the third. As mentioned above, the number of surfaces in the system could be reduced enhancing visibility of the fringes. It has been suggested

that some of the limitations of moiré techniques when applied to human topography are 1)size and depth requirements, 2)exposure time to living tissue, and 3) contrast loss on living tissue.[11] Other researchers have pointed out some of the advantages of the moiré technique when using reflective surfaces.[12] Because the cornea provides this advantage, the light intensity necessary is less and the contrast of the fringes greater. Studies involving the relationship between adjustment of the reference grating image and the test grating image have shown that by the necessary adjustment, the average plane of observation, (thus any asymmetry) can be determined.[13] If the target is a series of concentric circles instead of the traditional Ronchi ruling, the test lens position can be varied until any asymmetry is neutralized. The astigmatic axis then becomes easily visible in the moiré pattern produced by such a target. In this study, the alignment was controlled by observer judgment of symmetry within the reticle image. The more complicated surface of a human cornea requires more complicated targets for alignment to be precisely controlled. If the fixation point producing maximal symmetry is measured relative to the concentric ring target, the position of the corneal apex can easily be determined. When the target grating is 25 mm in diameter, using the vergences in figure 1, the area of the analogue being measured is approximately 12.6 mm^2. Aberrations as seen in this system which utilizes biconvex lenses reduces the effective area of the test analogue to approximately 7 mm^2. Correction for aberration would improve this situation. Lastly, by reducing the distances between the optical elements, the area of the test surface could be increased.

Figure 6 shows a moiré system adapted to a biomicroscope. This system reduces the distance between the optical elements and incorporates a concentric ring target. An observer can go directly from a microscopic analysis of the anterior cornea to a moiré analysis of the corneal topography by using a rotatable arm to swing the device into the path of observation. Yoshino, et al, have reported that zeroth order filtering doubles fringe visibility.[14] Their technique of fringe enhancement consists in

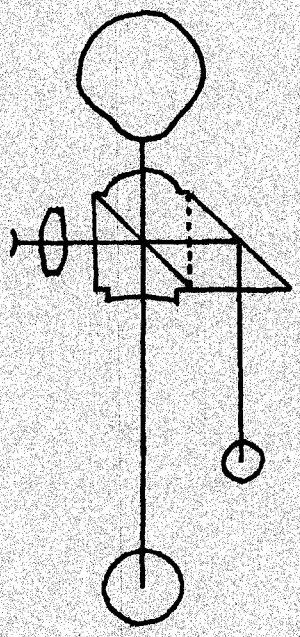

Figure 6

placing a stop in the plane of the exit port of the moiré apparatus. The spatial filtering effect can then serve as the observation criterion needed to calibrate and take measurements with the instrument. Also, the area of the cornea measured is no longer limited by aberrations because the spatial filter includes these factors. When the appropriate lens diameters are used, the exit port of the moiré device is in the plane of the plano concave lens shown in figure 6 and a 40 mm^2 area of the cornea can be measured at one time! The standard deviation of findings would perhaps differ from that obtained in this study. However, the relationship between reference lens position and test surface radius of curvature would remain the same.

The major advantages of this method of moiré corneal assessment are the compact construction, the direct readability of the findings, and the accuracy obtained with proper use of the instrument. One standard deviation corresponds to .03 mm radius of curvature! Further advantages of this technique are as follows: 1)readings can

be obtained quickly and accurately, 2)the instrument does not require much maintenance, and 3)patient discomfort is negligible. In summary, the method presented in this paper can be easily adapted to a biomicroscope utilizing the microscope system for observations and the slit lamp system for illumination of the target grating. It is anticipated that moiré methods will eventually replace present methods of determining corneal topography by providing a more compact and precise instrument that can be easily included in any eye examination.

REFERENCES

1. Ludlam, W., and M. Kaye, "Optometry and the New Metrology," Am. J. Opt. Arch. Am. Academy Opt. August:525-528,(1966).

2. Meyer-Arendt, J. R., "Testing of Glass Surfaces by an Incident Light Schlieren Method," J. Opt. Soc. Am. 46:1090-1091,(1956).

3. Meyer-Arendt, J. R., and E. D. Miner Jr., "Angular measurements by Means of a Ronchi Ruling," Applied Optics. 2:77,(1963).

4. Oster, G., M. Wasserman, and C. Zwerling, "Theoretical Interpretations of Moiré Patterns." J. Opt. Soc. Am. 54:169-175,(1964).

5. Yoshino, Y., and H. Takasaki, "Doubling Visibility Enhancement of Moiré Fringes of the Summation type," Applied Optics. 15:1124-1126,(1976).

6. Takasaki,H., "Moiré Topography," Applied Optics. 9:1457-1472,(1970).

7. Canal, A., G. Ranninger, and G. Windischbauer, "Shadowless Moiré Topography Using a Single Source of Light," Applied Optics. 13:722-723,(1974).

8. Ludlam, W., et. al., Am. J. Opt. Arch. Am. Academy Opt. August:525-528,(1966).

9. Chander, M., M.M. Bindal, A. Kulshreshtha, and B. K. Agarwala, "Photokeratography Using Moiré Techniques." Applied Optics, 15:2964-2965,(1976).

10. Mandel, R. D., "Corneal Curvature Measurements by the Aid of Moiré Fringes," J.O.A. J. 37:219-220,(1966).

11. Takasaki, H., "Moiré Topography," Applied Optics. 12:845-850,(1973).

12. Chiange, C., "Moiré Topography," Applied Optics. 14:177-179,(1975).

13. Yoshino, Y., M. Tsukiji, and H. Takasaki, "Moiré Topography by Means of Grating Hologram," Applied Optics. 15:2414-2416,(1976).

14. Yoshino, Y., et. al., Applied Optics. 15:1124-1126,(1976).

INDEX - RAW DATA

I. Test lens dimensions-

Back focal length = 19 mm $\pm$ .5 mm, therefore +52.632 D

Front focal length = 19 mm $\pm$ .5 mm, therefore +52.632 D

Center thickness = 10.3 mm $\pm$ .1 mm

Edge thickness = 2.3 mm $\pm$ .1 mm

Assumption - Lens is biconvex, therefore each surface has same power, P. Also, n = 1.523

$$+52.632 = \frac{P}{1 - P\frac{.0103}{1.523}} + P \text{ , thus } P = +23.991 \text{D/surface}$$

Equivalent power = $2(+23.991) - (.00676)(+23.991)^2 = \underline{+44.091 \text{ D}}$

Distance measured between front edge of test lens and cube face = 18 mm

Distance between cube face and principal plane of lens = 18 - .32 = 17.68 mm

II. Reference lens dimensions-

Back focal length = 19 mm $\pm$ .5 mm, therefore +52.632 D

Front focal length = 19 mm $\pm$ .5 mm, therefore +52.632 D

Center thickness = 10.8 mm $\pm$ .1 mm

Edge thickness = 2.7 mm $\pm$ .1 mm

Assumption - Same as for test lens calculations

$$+52.632 = \frac{P}{1 - P\frac{.0108}{1.523}} + P \text{ , thus } P = +23.907 \text{D/surface}$$

Equivalent power = $2(23.907) - (.00709)(23.907)^2 = \underline{+43.761 \text{ D}}$

Distance between reference lens edge and cube face = d

Distance between cube face and reference lens principal plane = d - .2

III. Telescope dimensions-

Distance measured between front of telescope and object being viewed through the telescope = 645 mm $\pm$ 1 mm

Distance measured between front of telescope and cube face when taking measurements = 42.5 mm $\pm$ .5 mm

IV. Cube beam splitter dimensions-

Thickness of cube = 25.0 mm $\pm$ .1 mm , n=1.515

note: Ronchi ruling target was in contact with the cube beam splitter.

V. Contact lens dimensions -

Reference contact lens anterior radius of curvature = r_o = 7.45 mm $\pm$ .05 mm

Test contact lenses anterior radii of curvature $\pm$ .05 mm

r_1 = 7.78 mm r_2 = 8.14 mm r_3 = 8.46 mm

VI. Reference lens position data -

Distance between cube surface and edge of lens when carriage position = 0.000 mm, d_o = 10.0 mm $\pm$ .5 mm

Distance between cube surface and edge of lens when image of Ronchi ruling, located in the plane of the telescope eyepiece reticle, has frequency of one reticle unit (position of unit magnification) d_u = 76.3 mm $\pm$ .5 mm

Raw data:

	carriage setting		
	d_1	d_2	d_3
1	20.421	14.555	7.946
2	19.774	13.932	6.307
3	19.881	13.035	7.558
4	20.366	13.642	6.943
5	20.529	14.624	7.152
6	19.577	13.298	7.449
7	20.833	13.669	8.111
8	20.981	14.091	8.107
9	20.143	14.469	8.170
10	21.039	13.595	7.237
11	21.386	13.629	8.267
12	20.767	13.650	7.111
13	20.573	13.181	7.337
14	20.252	13.773	6.414
15	20.187	13.845	7.335
16	19.714	13.181	6.051
17	21.536	14.753	7.100
18	20.617	15.169	6.936
19	19.875	14.204	7.814
20	20.010	13.425	6.724
$\bar{x}$	20.188	13.489	7.318
σ	.565	.581	.639